CHAPTER 3. MODEL OF THE SYSTEM

This chapter introduces the model of the system that represents the formation flight. The use of accurate dynamic models of aircraft and reliable meteorological forecast is mandatory in order to improve the predictability of the trajectories and obtain realistic estimations of the fuel savings. First, the dynamic model used to represent aircraft in solo flight is presented, together with the path constraints. Later, the dynamic model used to represent aircraft in formation flight is described. After that, the wind model is presented. Finally, the model of the direct operating costs of airlines is discussed.

3.1. Solo flight model

In aircraft trajectory optimization problems developed within the ATM context, a three degrees of freedom point-mass dynamic model of the aircraft is usually employed. In this model, the aircraft is represented as a point with variable mass due to the fuel consumption, moving in a four-dimensional space characterized by the three spatial dimensions together with time.

In this section, first, the reference systems are introduced. Later, some usual assumptions made to build an aircraft model to be used in the ATM context are described. After that, some simplifications are introduced to the model. Finally, the flight envelope is presented.

3.1.1. Reference systems

Several specific reference systems are used in flight mechanics to represent the elements involved in the motion of the aircraft, such as forces, torques, and velocities. The aim of these reference systems is to obtain practical expressions of the kinematic and dynamic equations of the aircraft [Tierno et al., 2012]. The reference systems of interest are the following: the Earth-Centered, Earth-Fixed (ECEF) reference frame, the local horizon reference frame, and the wind-fixed reference frame.

ECEF reference frame

The ECEF reference frame, F_{ECEF} as its name suggests, is a geocentric system, the axes of which are fixed with respect to the Earth's surface and rotate with the Earth. In particular, its origin is the center of gravity of the Earth and its axes are defined as follows: the x axis, x_{ECEF}, points towards the intersection of the Equator and the Greenwich meridian; the z axis, z_{ECEF}, points towards the North Pole; and, finally, the y axis, y_{ECEF}, completes a right-hand-oriented axes system.

Local horizon reference frame

The local horizon reference frame, F_{LH}, has its origin at the center of mass of the aircraft and its axes are defined as follows: the z axis, z_{LH}, points towards the center of the Earth; the x axis, x_{LH}, is contained in a horizontal plane and points towards a fixed direction of it, in this case, the north direction; and, finally, the y axis, y_{LH}, is also contained in a horizontal plane completing a right-hand-oriented axes system, pointing therefore towards the east direction.

Wind-fixed reference frame

To define the wind-fixed reference frame, the following assumption is made:

Assumption A: The aircraft has a plane of symmetry.

Thus, the wind-fixed reference frame, F_{WF}, is an aircraft-centered system, the axes of which rotate with the airspeed vector. In particular, its origin is the center of mass of the aircraft and its axes are defined as follows: the x axis, x_W, is aligned with the airspeed vector; the z axis, z_W, is contained in the plane of symmetry of the aircraft, orthogonal to x_W, and points downward in the usual flight attitude; and, finally, the y axis, y_W, is orthogonal to the plane of symmetry of the aircraft, completing a right-hand-oriented axes system.

The local horizon reference frame, F_{LH}, can be obtained from the ECEF reference frame, F_{ECEF}, through the rotations defined by the well known Euler angles, i.e., three consecutive rotations in the three-dimensional Euclidean space in a particular order, in this case, following the Tait-Bryan conversion, the order is z-y-x. Before performing these rotations, a translation is needed in order to make the origins of both reference systems match.

Similarly, the wind-fixed reference frame can be easily obtained from the local horizon reference frame by using the rotations defined by the Euler angles. For further information about the reference frames or about Euler's rotation theorem, please see [Hull, 2007].

3.1.2. Modeling assumptions

The following modeling assumptions are usually introduced in ATM-related studies [Hull, 2007, Tierno et al., 2012].

The first assumption comes from considering the ECEF reference system as an inertial reference system which is actually a non-inertial reference system.

Assumption B: The Earth is considered flat, nonrotating and the ECEF reference frame can be considered inertial.

Other modeling assumptions made in this thesis are the following:

Assumption C: The Earth is approximated as a sphere. In addition, typical aircraft cruise altitudes mean the acceleration due to gravity can be safely considered as a constant value: $g = 9.81\ m/s^2$.

Assumption D: The vertical component of the wind speed is considered to be negligible. Dynamic effects of wind are neglected.

Assumption E: All dynamic effects associated with elastic deformations, degrees of freedom of articulated subsystems such as flaps or rudders, or kinetic momentum of rotating subsystems with respect to the aircraft are neglected.

Assumption F: The only external forces acting on the aircraft are the propulsive, aerodynamic, and gravitational forces.

As a consequence of the former hypotheses, the aircraft is considered as a rigid solid with six degrees of freedom. The set of differential equations involving forces and torques that describes the dynamics of the aircraft should be solved simultaneously. However, the following assumption is introduced to simplify the solution:

Assumption G: Control surface deflections have quite lower effects on the aerodynamic forces than the corresponding effects on the aerodynamic torques.

This assumption allows forces and torques scalar equations to be decoupled leading to a three degrees of freedom point variable-mass dynamic model of the aircraft. Additional hypotheses made in this thesis are the following:

Assumption H: Since most jet airplanes have engines rigidly coupled with the aircraft structure, aircraft are assumed to have fixed engines in this thesis.

Assumption I: The aircraft is considered as a point variable-mass, as can be seen in the fuel mass flow equation. However, the low rate of variation of the mass of the aircraft leads it to be considered as a constant for the derivation of the kinematics and dynamics equations of motion.

Assumption J: A symmetric and coordinated flight is assumed and, hence, the airspeed vector, the propulsive forces and the aerodynamic forces are contained in the plane of symmetry of the aircraft.

Assumption K: A small thrust angle of attack is considered.

Fig. 3.1. Frontal, top, and lateral views of the aircraft together with the forces acting on it.

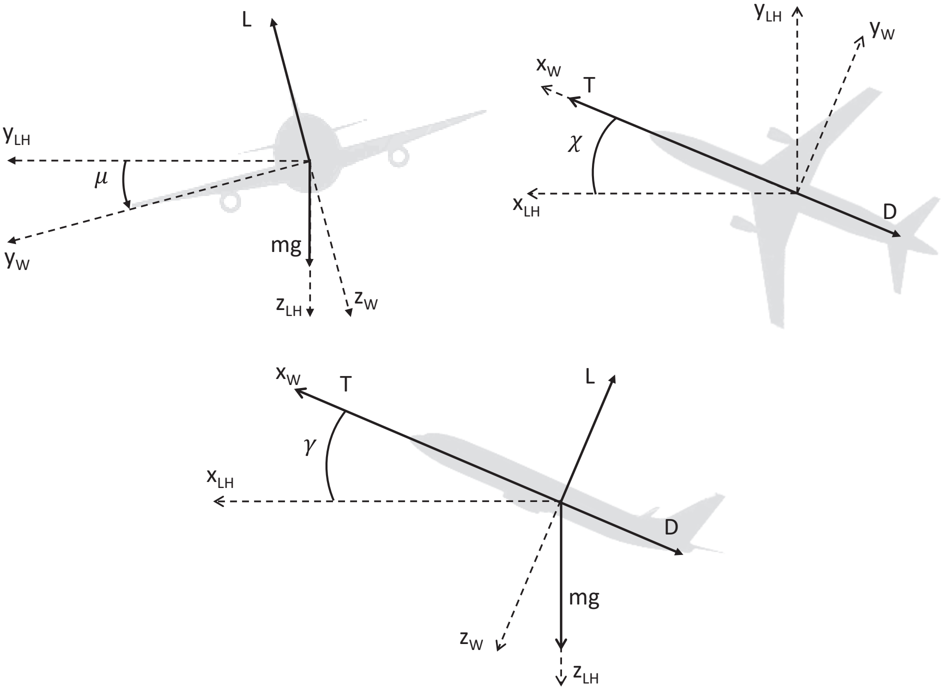

Considering the above assumptions and expressing the Euler's rotation using the Tait-Bryan convention for the wind-fixed reference frame with respect to the local horizon reference frame, the following angles will be used in the dynamics model of the aircraft:

- The heading angle, x, ($0 \leqslant x \leqslant 2\pi$), defined as the angle between the x_{LH} axis and the airspeed vector projection on the horizontal plane.

- The flight path angle, y, ($-\pi/2 \leqslant \gamma \leqslant + \pi/2$), defined as the angle between the airspeed vector and its projection on the horizontal plane.

- The bank angle, μ, ($-\pi \leqslant \mu \leqslant + \pi$), defined as the angle between the yw axis and the ($yw - zw$) plane intersection with the horizontal plane.A schematic representation of the forces acting on an aircraft together with the heading, flight path, and bank angles is given in Fig. 3.1.

3.1.3. Equations of motion

Taking into account the above assumptions, the motion of the aircraft can be described as a three degrees of freedom point variable-mass dynamic model defined by three dynamic equations, three kinematic equations, and one equation describing the fuel consumption flow rate. The equations of motion are hence defined by the following ordinary differential equations (ODE) system:

$$
\begin{aligned}
\dot{\phi} &= \frac{V\cos\chi\cos\gamma + V_{W_N}}{R_E + h}, \\
\dot{\lambda} &= \frac{V\sin\chi\cos\gamma + V_{W_E}}{\cos\phi\cdot\left(R_E + h\right)}, \\
\dot{h} &= V\sin\gamma, \\
m\dot{V} &= T - D - mg\sin\gamma, \\
-mg\cos\gamma\sin\mu &= mV(\dot{\gamma}\sin\mu - \dot{\chi}\cos\gamma\cos\mu), \\
L - mg\cos\gamma\cos\mu &= mV(\dot{\gamma}\cos\mu + \dot{\chi}\cos\gamma\sin\mu), \\
\dot{m} &= -T\eta,
\end{aligned}
\tag{3.1}
$$

where φ, λ, and h are the three-dimensional position variables, latitude, longitude, and altitude, respectively, V is the true airspeed, χ represents the heading angle, γ represents the flight path angle, and m is the mass of the aircraft. T is the thrust force and μ the bank angle. The lift force is $L = qSC_L$, where $q = \frac{1}{2}\rho V^2$ is the dynamic pressure, ρ is the air density, and S is the reference wing surface area. The aerodynamic drag force is $D = qSC_D$, where C_D is the drag coefficient. R_E is the Earth's radius.

A relationship between both aerodynamic coefficients, C_L and C_D, exists, which is known as drag polar, that is $C_D = C_D(C_L)$. In this thesis, the following assumption about the drag polar has been made.

Assumption L: A parabolic drag polar is assumed.

Hence, considering Assumption L, a parabolic drag polar can be expressed as: $C_D = C_{D0} + KC^2L$, where C_{D0} is the zero-lift drag component and K is the induced drag coefficient.

Other parameters and variables include the Earth's radius R_E and the gravitational acceleration g. V_{WE} and V_{WN} are the components of the wind velocity vector in eastward and northward directions, respectively. η is the thrust-specific fuel consumption. In particular, using Eurocontrol's base of aircraft data (BADA)[1] performance model for jet engines, the following equation applies:

$$\eta = C_{f1}\left(1+\frac{V}{C_{f2}}\right), \tag{3.2}$$

where C_{F1} and C_{F2} are empirical thrust-specific fuel consumption coefficients.

The BADA performance model provides accurate aircraft performance modeling such as fuel consumption, aerodynamic performance, and speed model, among others, for several types of commercial aircraft along different flight segments. Additionally, flight envelope information is also provided. Two families of aircraft performance modeling are available: BADA Family 3 and the newest BADA Family 4. In this thesis, BADA version 3.6 [Eurocontrol, 2013] has been used.

In general, the state and control variables are functions of time. The aerodynamic forces, L and D, are functions of their aerodynamic coefficient as well as of the atmospheric variables such as the density of the air ρ and the true airspeed of the aircraft V. Likewise, atmospheric variables depend on the position of the aircraft. Additionally, using the drag polar relationship, the relation between both aerodynamic coefficients can be taken into account. Finally, the components of the wind field depend on the position of the aircraft. For the sake of simplicity of the exposition, all these functional dependencies have been omitted.

Rearranging the last two dynamic equations in the ODE system (3.1), the explicit expressions for $\dot{\Upsilon}$ and $\dot{\chi}$ can be obtained, producing the following equivalent ODE system:

[1] https://www.eurocontrol.int/model/bada

$$\begin{aligned}
\dot{\phi} &= \frac{V\cos\chi\cos\gamma + V_{W_N}}{R_E + h}, \\
\dot{\lambda} &= \frac{V\sin\chi\cos\gamma + V_{W_E}}{\cos\phi\cdot\left(R_E + h\right)}, \\
\dot{h} &= V\sin\gamma \\
\dot{V} &= \frac{T - D - mg\sin\gamma}{m}, \\
\dot{\chi} &= \frac{L\sin\mu}{mV\cos\gamma}, \\
\dot{\gamma} &= \frac{L\cos\mu - mg\cos\gamma}{mV}, \\
\dot{m} &= -T\eta,
\end{aligned} \tag{3.3}$$

where the state vector has seven components: the three dimensional position variables, φ, λ, and h, the true airspeed V, the heading angle χ, the flight path angle γ, and the mass of the aircraft m. In this set of equations, the control vector has three components: the thrust force T, the lift coefficient C_L, and the bank angle μ Thus, for aircraft p, the state vector is x_p _ (φ_p, λ_p, h_p, V_p, $\chi_p \gamma_p$, m_p), $\forall$ p ϵ {1 ,...,N_a}, and the control vector is u_p _ (T_p, C_{Lp} ,μ_p), $\forall$ p ϵ {1,..., N_a}, with N_a the number of aircraft involved in the mission design problem.

3.1.4. Flight Envelope

Flight envelope constraints represent aircraft performance limitations. These constraints make reference to flight altitude, load factor, and airspeed, among others, and they can be stated in the form $\eta L(t) \leq \eta(t) \leq \eta u(t)$, where η is the state or control variable and nL and η_u are the minimum and maximum allowed values of the variable, respectively. The BADA has been employed again to impose the following constraints:

$$\begin{aligned}
V_{min} \leq \quad & V_{CAS} \leq \quad V_{MO}, \\
m_{min} \leq \quad & m \leq \quad m_{max}, \\
& M \leq \quad M_{MO}, \\
T_{min} \leq \quad & T \leq \quad T_{max}, \\
C_{Lmin} \leq \quad & C_L \leq \quad C_{Lmax},
\end{aligned} \tag{3.4}$$

where V_{CAS} is the calibrated airspeed, V_{min} and V_{MO} are the minimum and maximum operating calibrated speeds, respectively, m_{min} and m_{max} are the minimum and maximum aircraft masses, respectively, M is the Mach number and M_{MO} is the maximum operating Mach number, T_{min} and T_{max} are the minimum and maximum available engine thrusts, respectively, and C_{Lmin} and C_{Lmax} are the minimum and maximum lift coefficients, respectively. Finally, μ_{max} is the maximum bank angle set by the air navigation regulations in civil flight. Furthermore, the BADA includes the equation $V_{min} = Cv_{min} V_s$, where Cv_{min} is the minimum speed coefficient and V_s is the stall speed for each flight phase.

The V_{CAS} can be calculated as a function of the true airspeed V_{TAS} [Eurocontrol, 2013], by the following expression:

$$V_{TAS} = \left[\frac{2}{\upsilon} \frac{p}{\rho} \left\{ \left(1 + \frac{p0}{p} \left[\left(1 + \frac{\upsilon}{2} \frac{\rho 0}{p0} V_{CAS}^2 \right)^{1/\upsilon} - 1 \right] \right)^{\upsilon} - 1 \right\} \right]^{0.5}, \tag{3.5}$$

where p is the air pressure, ρ is the air density, and p_0 = 101325 Pa and ρ_0 = 1.225 kg/m^3 are the air pressure and the air density at mean sea level (MSL), respectively. Finally, υ is defined as $\upsilon = \frac{\kappa - 1}{\kappa}$, where κ = 1.4 is the adiabatic index of air.

For turbofan-propelled aircraft, assuming standard atmosphere conditions, the maximum thrust T_{max} is defined by the following empirical expression:

$$T_{max} = C_{T_{cr}} \cdot C_{T_{C,1}} \cdot \left[1 - \frac{H_p}{C_{T_{C,2}}} + C_{T_{C,3}} \cdot H_p^2 \right], \tag{3.6}$$

where C_{Tcr} is the maximum cruise thrust coefficient, $C_{Tc,1}$, $C_{Tc,2}$, and $C_{Tc,3}$ are the empirical thrust coefficients, and H_p is the geopotential pressure altitude.

3.2. Formation flight aircraft dynamics

The differential algebraic equations (DAE) system (3.3) is applicable to any aircraft in any phase of solo flight. However, depending on the aircraft type, the aerodynamic coefficients, the wingspan, and the reference surface, among others, the parameters of this DAE system change. In formation flight, further modifications must be introduced into the dynamic equations of the trailing aircraft.

As stated in Chapter 2, extended formations are intrinsically safer than close formations, which is why only extended formations have been considered in this thesis. In extended formations, aircraft fly with a longitudinal separation of more than 10 wingspans but the potential fuel burn reduction for the trailing aircraft has a significant decrease beyond 20-wingspans'separation. Therefore, in this thesis, the formation benefits are considered negligible for separations of more than 20 wingspans and the constraint introduced to model the distance which leads to fuel burn reductions in the trailing aircraft during formation flight is the following:

$$10b \leq D_{pq} \leq 20b, \qquad \forall p,q \in \{1,\dots,N_a\}, p<q, \tag{3.7}$$

where b is the wingspan of the leader aircraft and D_{pq} is the great-circle distance between aircraft p and q at time t.

The haversine formula has been used to determine the great-circle distance D between two points given their latitudes and longitudes:

$$D = 2R_E \arcsin\left(\sqrt{\sin^2\left(\frac{\phi q - \phi p}{2}\right) + \cos\left(\phi_p\right)\cos\left(\phi_p\right)\sin^2\left(\frac{\lambda_q - \lambda_p}{2}\right)}\right), \tag{3.8}$$

where (φ_q, λ_q) and (φ_p, λ_p) are the latitude and longitude of aircraft q and p, respectively, at any time.

As mentioned in Chapter 2, due to the formation flight, a significant decrease in induced drag is achieved for the trailing aircraft. According to Assumption L, the expression of the parabolic drag polar is

$$C_D = C_{D0} + C_{Di,} \tag{3.9}$$

where C_{D0} is the parasitic drag, which represents the aerodynamics clean performance of the aircraft, and C_{Di} is the induced drag, that is, the drag component due to lift. The induced drag can be expressed by

$$C_{Di} = \frac{C_L^2}{\pi \cdot AR \cdot e} = KC_L^2, \tag{3.10}$$

where $AR = b^2/S$ is the aspect ratio, e is an efficiency factor, which will be equal to the unity for elliptical lift distribution and lower than the unity for any other distribution, and

Table 3.1: Longitudinal distance constraints and parabolic drag polar in solo and formation flights.

Solo flight	Formation flight
$D_{pq} \geq 20b$	$10b \leq D_{pq} \leq 20b$
$C_D = C_{D0} + KC^2_L$	$C_D = C_{D0} + (1 - \epsilon)\ KC^2_L$

$K = 1/(\pi \bullet AR \bullet e)$ is the lift-induced drag coefficient.

As mentioned in Chapter 2, due to formation flight, a significant decrease in the induced drag, KC^2_L, is achieved for the trailing aircraft, hence, the parabolic drag polar for a trailing aircraft flying in a formation can be expressed as [Hartjes et al., 2018], [Hartjes et al., 2019]

$$C_D = C_{D0} + (1 - \in) KC_L^2, \tag{3.11}$$

where ϵ represents the rate of induced drag reduction achieved for the trailing aircraft. The value of ϵ is highly dependent on the type of aircraft involved in the formation, the streamwise and the lateral distance between aircraft, the type of formation flight, and the wind, among others. According to [Ning, 2011], in which a zero wind field has been assumed, a maximum reduction in the induced drag of 30±3% is achieved in a two-aircraft formation and a maximum reduction in the induced drag of 40 ± 6% in a three-aircraft formation (95% confidence intervals).

Therefore, during formation flight, the dynamics model of the leader aircraft is represented by the ODE system (3.3) with the standard parabolic drag polar, whereas the dynamic model of the trailing aircraft is represented by the same set of equations but replacing the standard parabolic drag polar by Eq. (3.11). The selection of the form of the drag polar is made based on the longitudinal distance between aircraft, as schematically illustrated in Table 3.1.

Considering that aircraft will not join in formation during the take-off, landing, and approach phases of flight [Hartjes et al., 2018], in the mission design problem studied in this thesis, only the cruise phase of the flights is considered. Moreover, the motion of the aircraft involved in the formation flight is restricted to the horizontal plane at cruise flight level, not allowing changes in the flight level. Thus, in addition to the assumptions of Section 3.1, the following assumption is made:

Assumption M: The flight path angle is zero, $\gamma = 0$.

Considering Assumption M, the dynamic models of the aircraft can be simplified. The resulting simplified model is a two degrees of freedom point variable-mass dynamic obtained by substituting $\gamma = 0$ in the DAE system (3.3). The motion of the aircraft restricted to the horizontal cruise plane is described by the following set of kinematics and dynamics DAE:

$$\begin{aligned}
\dot{\phi} &= \frac{V\cos\chi + V_{W_N}}{R_E + h}, \\
\dot{\lambda} &= \frac{V\sin\chi + V_{W_E}}{\cos\phi \cdot (R_E + h)}, \\
\dot{V} &= \frac{T - D}{m}, \\
\dot{\chi} &= \frac{L\sin\mu}{mV}, \\
\dot{m} &= -T\eta,
\end{aligned} \tag{3.12}$$

together with the following algebraic equation:

$$L = \frac{mg}{\cos\mu}, \tag{3.13}$$

where the state vector has only five components, two less than DAE system (3.3): the two dimensional position variables, latitude and longitude, denoted by φ and λ, respectively; the heading angle χ; the true airspeed V; and the mass of the aircraft m.

In this set of equations, the control vector formally includes three components: the thrust force T, the lift coefficient C_L, and the bank angle μ. However, two control variables are directly related due to the requirement of equilibrium of forces given by Eq. (3.13) and, therefore, the number of control variables is two. Thus, for aircraft p, the state vector is $x_p = (\varphi_p, \lambda_p, V_p, \chi_p, m_p)$, $\forall\, p \in \{1,\dots,N_a\}$, and the control vector is $u_p = (T_p, \mu_p(C_{Lp}))$, $\forall p \in \{1,\dots, N_a\}$, with N_a the number of aircraft involved in the mission design problem.

Note that, for problem conditioning and numerical stability, normalized versions of both the DAE system (3.12) and Eq. (3.13) have been used in this thesis in the numerical experiments described in chapters 7 and 8.

Concerning the formation flight modeling, the following assumption has been adopted:

Assumption N: The benefits obtained by flying in a formation are modeled as a rate of reduction in fuel burn consumption.

Considering Assumption N, the fuel savings factor can be directly introduced in the last differential equation of the DAE system (3.12) instead of considering the reduction in the induced drag. With $\mathfrak{R}_{\text{fuel}}$ being the rate of reduction in fuel burn consumption due to the formation flight, the mass flow rate equation for the trailing aircraft during the formation flight can be expressed as

$$\dot{m} = -\left[1 - \mathfrak{R}_{\text{fuel}}\right] \cdot T \cdot \eta. \tag{3.14}$$

A schematic description of the differences between the flight models employed in this

Table 3.2: Longitudinal distance constraints and dynamic model in solo and formation flights.

Solo flight	Formation flight
$D_{pq} \geq 20b$	$10b \geq D_{pq} \geq 20b$
$\dot{\phi} = \dfrac{V\cos\chi + V_{W_N}}{R_E + h}$,	$\dot{\phi} = \dfrac{V\cos\chi + V_{W_N}}{R_E + h}$,
$\dot{\lambda} = \dfrac{V\sin\chi + V_{W_E}}{\cos\phi \cdot (R_E + h)}$,	$\dot{\lambda} = \dfrac{V\sin\chi + V_{W_E}}{\cos\phi \cdot (R_E + h)}$,
$\dot{V} = \dfrac{T - D}{m}$,	$\dot{V} = \dfrac{T - D}{m}$,
$\dot{\chi} = \dfrac{L\sin\mu}{mV}$,	$\dot{\chi} = \dfrac{L\sin\mu}{mV}$,
$\dot{m} = -T\eta$,	$\dot{m} = -\left[1 - \mathcal{R}_{\text{fuel}\dagger}\right] \cdot T \cdot \eta$,
$L = \dfrac{mg}{\cos\mu}$,	$L = \dfrac{mg}{\cos\mu}$

thesis to describe the solo and formation flights is given in 3.2. The model is selected based on the longitudinal distance between aircraft.

It is quite difficult to model the drag reduction ϵ and, hence, the fuel burn reduction $\mathfrak{R}_{\text{fuel}}$ achieved during a formation flight, since there are many factors to take into account. The number of aircraft involved in the formation, their type, size, and weight, the ability of the trailing aircraft to place itself in the optimum location of the wake, and the stresses and vibrations induced, among others, strongly influence the benefits of the formation.

It is important to point out that the full three degrees of freedom point variable-mass dynamic model described in the DAE system (3.3) with the induced drag reduction modeling described by Eq. (3.11) could have been employed in the formation mission planner presented in this thesis. However, using the full model makes the statement of the problem, its numerical resolution, and the analysis of the results more complicated. For this reason, the reduced model has been used in this thesis.

Taking into account the assumptions made in this section, the obtained results are slightly less accurate. In particular, taking Assumption M and Assumption N into consideration may lead to a loss of accuracy in the speed profile and flight altitude. In [Ning, 2011], the aerodynamic performance of extended formations is analyzed in detail. The results show that aircraft within a formation fly at a slower cruise speed than in their respective solo flights, as this helps to achieve a reduction in the penalties associated with viscosity and compressibility effects induced by the formation flight. Consequently, aircraft within the formation would also need to fly at a lower altitude, at a higher lift coefficient, or a combination of both compared with solo flight. Therefore, aircraft in formation tend to cruise at a slightly lower speed than when flying solo, as shown in [Voskuijl, 2017], [Hartjes et al., 2018], and [Hartjes et al., 2019].

Other assumptions made in the formation mission design problem presented in this thesis regard the relative position of each aircraft, which is set in advance, and the type of formation allowed in three-aircraft formations, which is the in-line formation.

Finally, a maximum detour time from the solo flight time has been set in order to perform a more realistic formulation of the formation mission design problem, according to the usual operational requirements.

3.3. Wind model

ERA-Interim [Dee et al., 2011] is a third-generation global atmospheric reanalysis produced by the european centre for medium-range weather forecasts (ECMWF). Climate reanalysis consists in systematic and coherent assimilation of the global meteorological data constrained by the available observations obtained from different sources during the period of reanalysis, such as radiosondes or aircraft, and prior state estimates using an invariant consistent assimilation scheme and an integrated meteorological model. The third-generation reanalysis data refers to the last generation, which was developed in 2010s and significantly enhanced the spatiotemporal resolution of the former ones.

Gridded data products, which can be found in the ERA-Interim database, include a wide variety of atmospheric parameters relevant to the mission design problem such as air temperature, pressure, and wind at different altitudes and sea-surface temperatures. In this thesis, the components of the wind velocity in eastwards and northwards directions have been used.

ERA-Interim is presented as a regular latitude-longitude grid, with a spatial resolution from 0.25º x 0.25º to 3º x 3º for the deterministic reanalysis, at 37 atmospheric levels corresponding to different pressure levels from 1 to 1000 hPa. The temporal coverage is four times daily, returning six-hour data. In this study, the chosen pressure level was 200 hPa, corresponding to the cruise altitude. The selected spatial resolution was 0.5º x 0.5º. Finally, the selected day was April 30, 2019, at 12:00. To include atmospheric data in the hybrid optimal control problem used to solve the mission design problem, an analytic function that approximates the data must be determined. For this purpose, radial basis functions (RBF) [Buhmann, 2003] have been used.

The RBF technique approximates multivariate functions using the distance measure concept to obtain a function approximation from a set of known input data. In particular, given a set of known input data, a function approximation at any point is obtained constructing a linear space which depends on the relative position of the evaluated point with respect to the known observations according to an arbitrary distance measure. RBF consider interpolating functions of the form

$$F(x) = c_0 + \sum_{i=0}^{N-1} c_c \varphi\left(\|x - R_i\|\right), \tag{3.15}$$

where $x \in \mathbb{R}^N$ is the input data vector and N is its dimension, $F(x)$ is the function approximation, φ is the basis function, and R_i is a vector containing the centers, which are the reference points of the basis functions. c_0 and c_c are constant coefficients calculated by the RBF method, in particular, c_0 is the bias term. The Euclidean norm is used to compute the distance between the input points and the centers. There are different options for the choice of the basis functions. In this thesis, Gaussian basis functions have been selected, expressed as follows:

$$\varphi(x) = e^{\left(-x^2/2\sigma\right)}, \tag{3.16}$$

where σ is a scaling parameter.

Fig. 3.2. Eastward wind speed on April 30, 2019 at 12:00.

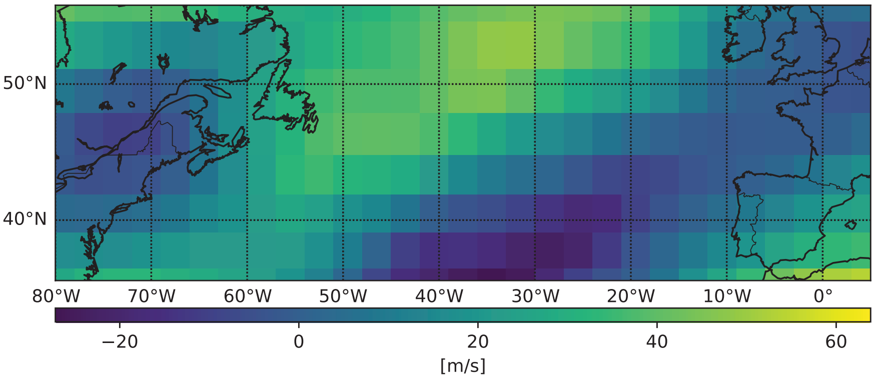

Eastwards and northwards components of the wind speed taken from ERA-Interim and then approximated by the RBF method are represented in Fig. 3.2 and Fig. 3.3, respectively.

3.4. Model of the direct operating costs

According to the different operational functions within an airline, the costs can be classified into three major groups [Camilleri, 2018, ICAO, 2017]: flight operating costs, ground operating costs, and system operating costs. Any expense related to the operation of the aircraft is included in the flight operating costs, for example flight crew salaries, maintenance and fuel and oil expenses as well as aircraft ownership, depreciation and amortization. Passenger handling, cargo handling, and aircraft servicing belong to the ground operating costs. Landing fees together with reservation and ticketing services expenses are also included

Fig. 3.3. Northward wind speed on April 30, 2019 at 12:00.

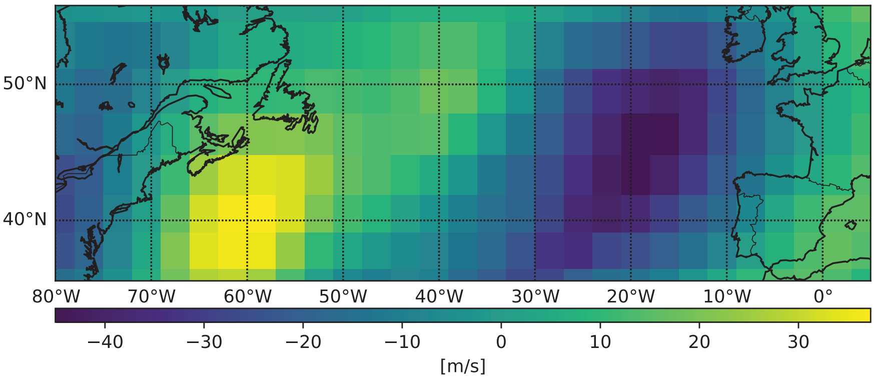

in this group. Finally, any corporate costs are included in the system operating costs. For instance, this applies to marketing and administrative costs, publicity costs, and on-board passenger services such as meals and entertainment. Fig. 3.4 gives a schematic categorization of the above costs. The historical percentage associated with flight operating costs is the greatest, amounting to half the total costs. Ground operating costs make up around 30% and, therefor esystem operating costs account for the lowest share of approximately 20%.

Fig. 3.4. Main functional expenses classified into flight, ground, and system operating costs.

Flight operating costs	Ground operating costs	System operating costs
Flight crew Fuel & oil Maintenance Aircraft ownership	Aircraft servicing Passenger handling Cargo handling Sales fees	Passenger services Advertising General Administrative

Direct operating costs, also known as DOC, are particularly important in trajectory optimization purposes, because not only do they represent a great rate of the whole costs of an airline, but they also depend critically on the performance of the flights. These expenses are usually divided into three different groups: flight operating costs such as flight crew salaries, fuel and oil, and airport and en-route charges; costs related to maintenance and overhaul; and aircraft depreciation. Fuel and oil consumption cost is of great importance since it represents about 20-30% of the total cost of an airline. Notice that several of the costs included in the DOC are indirectly time-related costs such as flight crew salaries, maintenance and overhaul, and aircraft depreciation.

The choice of the objective functional is decisive in any trajectory optimization problems in which the fuel consumption is, in general, minimized. However, two inherently competing criteria must be considered in formation mission design problems: fuel consumption and flight time. Indeed, on the one hand, formation flight, in general, reduces the total fuel consumption and, on the other hand, it usually requires an increase in the total flight time to create the formation itself. Therefore, the need to get away from traditional fuel consumption minimization criteria is clearly evident in formation mission design problems. Although costs related to the duration of the flight and to fuel consumption are both included in the DOC, evaluating the DOC as a whole is quite challenging because it entails modeling all the costs associated with aircraft flying operations, which is beyond the scope of this thesis. Therefore, instead of using the DOC, the cost index (CI) has been employed in the objective functional. The CI is defined as the ratio between time-related and fuel-related operational costs, C_{time} and C_{fuel}, respectively, for a specific flight as follows:

$$CI = \frac{C_{time}}{C_{fuel}}. \tag{3.17}$$

Choosing the CI based on the interests of the airlines for the flights involved in a formation mission makes it possible to obtain a solution that represents the desired balance between flight time-related and fuel-related operational costs.

In this thesis, fuel consumption and flight time are combined in the objective functional using weighting coefficients based on typical CI values. No other costs have been considered.

The objective functional J for N_a aircraft, is defined as follows:

$$\min \qquad J = \alpha_t \sum_{p=1}^{Na} t_{flight_p} + \alpha_f \sum_{p=1}^{Na} m_{f_p}, \tag{3.18}$$

where α_t and α_f are the time and the fuel burn weighting parameters, respectively, $t_{flightp}$, $\forall\, p \in \{1,\ldots, N_a\}$, is the total flight time for aircraft p, and mf_p, $\forall\, p \in \{1,\ldots, N_a\}$, is the fuel consumption for aircraft p.

It is worth mentioning that the initial fuel loaded into an aircraft that has good chances of benefitting from a formation flight could be considerably lower than the amount of fuel loaded into the same aircraft without good chances to benefit from a formation flight. Nevertheless, in this thesis, a more conservative approach has been adopted and all aircraft are loaded with the same amount of fuel as in solo flight, even if this factor will result in lower benefits in terms of DOC.

3.5. Conclusions

In this chapter, the model of the system that represents the formation flight has been introduced. It includes the wind model and the model of the direct operation costs of the flight based on typical cost index values, combining fuel consumption, and flight time. A detailed description of the modeling assumptions has been made. The main assumption is that formation flight is allowed only in the cruise phase of the flight, and, therefore, only this phase of the flight has been considered in the formulation of the formation mission design problem. Considering only this phase of the flight, in which aircraft fly in the horizontal plane, leads to a reduction of their dynamic models. Another important assumption is that the benefits achieved by the trailing and the intermediate aircraft due to the formation flight can be directly modeled as a rate of reduction in the fuel consumption instead of in the induced drag. Although accuracy is lost due to these assumptions, they lead to a simplification in the statement of the problem, its numerical resolution, and the analysis of the results. However, it is important to point out that the methodology employed in this thesis to solve the formation mission design problem could have been applied to the full model without introducing any simplification.